Fretting fatigue of interference fitted joints: development of a novel specimen for four-point rotating-bending tests and experimental results

FRETTING FATIGUE OF INTERFERENCE FITTED JOINTS: DEVELOPMENT OF A NOVEL SPECIMEN FOR FOUR-POINT ROTATING-BENDING TESTS AND EXPERIMENTAL RESULTS

D. Croccolo[a], M. De Agostinis[a], S. Fini[a], G. Olmi[a], L. Paiardini[a], F. Robusto[a]*, C. Scapecchi[a]

[a] Department of Industrial Engineering (DIN), University of Bologna, Viale del Risorgimento 2, 40136 Bologna, Italy

*francesco.robusto@unibo.it Tel. +39-051-2093334

Abstract: Interference-fitted joints are widely used to join a shaft and a hub. The contact pressure produced by the interference induces stress concentration on the shaft at the hub end. FEA can be helpful in evaluating the related stress concentration factor. However, fretting damage may be generated and may arise from micro-sliding between the mating surfaces. It is currently not feasible to take this occurrence into account and to properly and reliably address this phenomenon by a standard numerical simulation. In order to tackle this question, an ad hoc specimen was designed for four-point rotating bending fatigue testing. The new specimen has three main advantages: the first one is the reduced dimensions with respect to the usually tested shafts, the second is the possibility of controlling the average contact pressure, and the third is the capability of easily dismounting the specimen without damaging the coupled surfaces. The specimen has been then tested. The study focused on C40 normalized steel, whose fretting fatigue limit was experimentally evaluated by the aforementioned device. The mating surfaces could also be carefully analyzed for fretting damage detection after cycling. The fatigue limit retrieved was 254 MPa and fretting damage and induced cracks were detected in the specimens, which proves the effectiveness of the introduced testing rig at reproducing fretting fatigue damage.

Keywords: Interference joint, conical clamping, fretting fatigue, fretting damage,

List of symbols:

r_{Bi} : bushing internal radius [mm]

r_{BH} : hub-bushing mean radius [mm]

r_{He} : hub external radius [mm]

r_{Se} : shaft external radius [mm]

r : generic radius [mm]

p_{HB} : contact pressure between hub and bushing [MPa]

p_{BS} : contact pressure between bushing and shaft [MPa]

s : bushing axial displacement [mm]

α : conical coupling angle [°]

E_H : hub Young's modulus [MPa]

E_B : bushing Young's modulus [MPa]

E_S : shaft Young's modulus [MPa]

ν_H : hub Poisson's ratio [-]

ν_B : bushing Poisson's ratio [-]

ν_S : shaft Poisson's ratio [-]

Q_H : hub aspect ratio [-]

Q_B : bushing aspect ratio [-]

Q : bushing non-dimensional generic radius [-]

σ_r : bushing radial stress [MPa]

σ_t : bushing tangential stress [MPa]

z_{BS} : radial displacement [mm]

ε_t : tangential deformation [-]

$S_{n\_notched}$: notched specimens fatigue limit [MPa]

S_{n_plain} : plain specimens fatigue limit [MPa]

$\sigma_{notched}$: notched specimens' standard deviation [MPa]

σ_{plain} : plain specimens' standard deviation [MPa]

k_f : stress concentration factor for fatigue (notch factor) [-]

1. Introduction

Interference coupling and screw clamping are widely used to join a shaft to a hub. The joint fastening capability is strictly related to the achievable contact pressure at the shaft and the hub interface. In a screw fastener, this pressure can be fulfilled as an effect of the tightening force of one or more screws [1]. Another way to generate a contact pressure at the interface is by applying a certain amount of radial interference. In both cases, the coupling involves a radial deformation of the shaft [2,3]. However, the induced deformation acts as any other geometrical discontinuity and, therefore, in the presence of external loads, causes a local stress increase. Hence, the stress concentration may lead to component fatigue failures in the presence of cyclic loads. For instance, these failure modes may occur in the front forks of bikes or motorbikes [4], in railway axles [5–8], or in the field of oil and gas and turbines [9,10]. Other applications involve motor crankshafts [11], aeronautical engine blade turbines [12,13], and dovetail couplings [14–19].

When considering shaft-hub joints under a cyclic bending load, a relative displacement at the interface between the hub rounded end and the shaft may occur, triggering a damage mechanism known as fretting fatigue [20]. Failures due to fretting fatigue cracks propagation happen under the traditional fatigue limit in the component. This occurrence depends on a large number of parameters, making the design process difficult. Even though fretting fatigue has been studied since the 1920s [21], the topic is still of great interest. Many researchers are currently working on several aspects, such as the numerical simulation of fretting on heterogeneous materials [22,23], numerical simulation of fretting wear [24,25], the effect of treatments [26–30], design of testing fixtures [16,31,32]. Some authors have investigated the influence of fretting fatigue damage on railway axles, where a noticeable amount of failures is reported in the vicinity of the press-fitted region of the wheel-axle assembly [33–35]. However, running fatigue tests on real scale models is often time-consuming. Many of the press-fitted fretting fatigue specimens that have been used throughout the years are either remarkably largely sized [33,36–38] (with diameters ranging from 42mm to 192mm) or difficult to disassemble, which prevents the observation of cumulated fretting damage [39,40].

Therefore, Croccolo et al. developed a testing methodology to assess the fatigue response of shaft-hub interference-fitted joints involving reduced dimension specimens [41,42] to be loaded under four-point rotating bending. Running tests under rotating bending makes it possible to take advantage of simple and cheap testing machines that operate at relatively high frequencies. On the other hand, the specimen dimension needs a careful design, as it is strictly related to the available load capacity of the rotating bending machine. The previously developed specimen, described in [41], consisting of a shaft and a hub to be shrink-fitted, exhibited well-conceivable dimensions. However, a not-fixable issue arose from mating surfaces being damaged upon coupling and, especially, decoupling phases. In addition, the previously mentioned specimen, designed according to Standard ISO 1143 [43], exhibited an 11 mm coupling diameter at the interface between the shaft and the hub, corresponding to the sample gage. It is well known that the contact pressure is directly proportional to the specific interference. Therefore, for this diameter, working out an expected value of coupling pressure as a function of a controlled radial interference was likely to lead to a poor robustness issue. In particular, careful interference control would have required a particularly strict tolerance prescription, which would have been generally difficult to accomplish and thoroughly check. Consequently, little variations in radial interference would have occurred, which, in turn, would have yielded considerable variations of contact pressure. To properly address this issue, in this paper, the authors develop a new specimen that, using a conical coupling, allows for strict control of the contact pressure at the interface. A contact pressure analytical model that accounts for initial clearance is also developed. Moreover, the shaft and hub parts may be easily separated after the test, allowing to subsequently analyze the mating surface by microscope observations.

An experimental campaign has been carried out in order to evaluate the fatigue behavior of the notched specimens of C40 steel. The experimental campaign has been followed by the statistical processing of the retrieved results and some experimental tasks aimed at carefully analyzing fretting-induced surface wear and cracks. These additional studies have finally made it possible to validate the capability of the here presented testing rig to actually reproduce fretting fatigue damage.

2. Materials and methods

2.1 Design of the specimen

The specimen has been developed to be tested on the test benches available at the University of Bologna. In particular, the rotating bending test bench is the RB 35 manufactured by Italsigma S.r.l. of Forlì, Italy. Some technical data, which are concerned with specimen design specifications, are provided in the following. This machine can perform four-point rotating bending tests, according to [43]. The driving speed of the mandrel, actuated by an electric motor, can be live controlled up to a maximum value of n = 3600 rpm. The specimen is clamped between the drive and the driven mandrels (the latter is a free mandrel that supports the specimen). Both mandrels are hinged at the mainframe of the bench; during a test, the bending moment can be applied by a calibrated mass or an actuator, while the current number of cycles is monitored by a counter. Each mandrel consists of a threaded nut that, following proper tightening, can preload a tapered split collet, whose internal diameter bears one end of the specimen. The biggest collet available has an internal diameter of 16 mm, whereas the maximum allowable length is 250 mm. According to specimen geometry recommendations in [43], the gauge diameter must be smaller than that of the collet to be coupled to its head.

It is well known that for small diameters, even a slight variation in radial interference implies a significant fluctuation in terms of specific interference, which, in turn, leads to a remarkably high scattering affecting contact pressure. The impossibility of adequately controlling radial interference, which leads to a significant bias, was the most significant drawback of the previous shaft-hub specimen [41], whose drawing is shown in Figure 1, following complete assembly, for the sake of completeness.

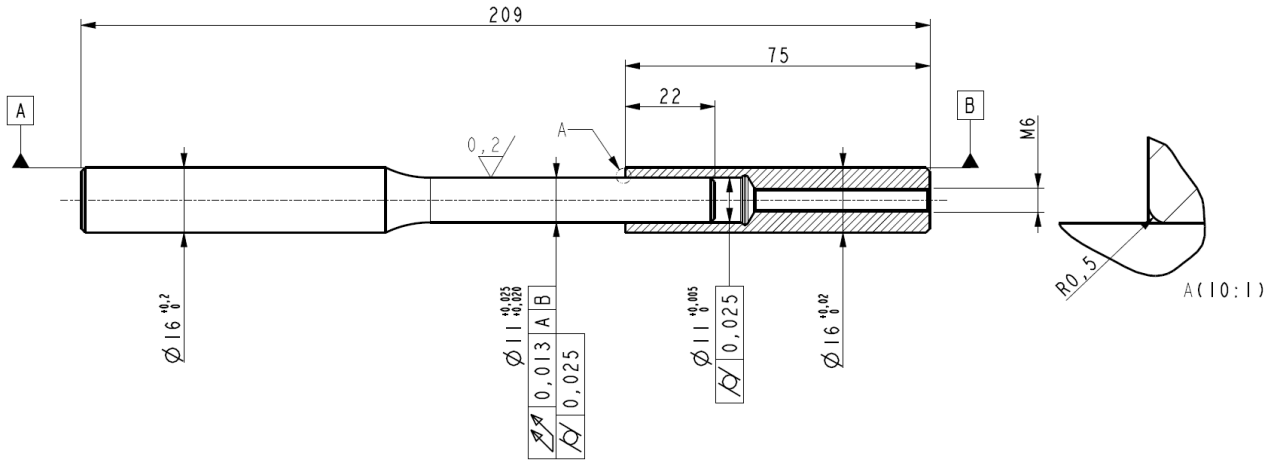

Figure 1 – Previous version of the specimen assembly [41] (not in scale, all dimensions in mm)

For this reason, in this study, a new specimen geometry, reproducing the notch at the shaft-hub coupling, has been conceived for tests under rotary bending fatigue. The new specimen, shown in Figure 2, takes inspiration from the previous specimen, achieving the required contact pressure using a tapered shaft-hub joint. In this coupling, the contact pressure is achieved as an effect of the interference induced by the controlled displacement between two conical elements (tagged as bushing and hub in Figure 2). The conical surfaces with a taper of 2% are pressed together, tightening the ring nut, thus generating radial forces. These forces provide the required pressure and, in turn, the needed frictional coupling between the hub and the shaft.

This device makes it possible to simulate a frictional coupling efficiently and reliably between a shaft and a hub involved in transmitting torques or forces. A further important point is that conical coupling keeps a relevant role in enabling an easy decoupling between the shaft and the hub. Untightening the ring nut, the pressure between the shaft and the hub drops to zero, and it is possible to disassemble the parts manually. Consequently, the shaft surface, as well as crack nucleation sites, are not damaged and, therefore, can be carefully analyzed, to investigate the presence of fretting-induced wear or cracks.

This procedure also allows insight not destructive control of the shaft surface (by penetrant liquids or other techniques), to detect fretting cracks before the specimen failure. For this purpose, in the present research, spray fluorescent dye penetrants were applied (QPL-USAF, which exhibits a yellow/green color under ultraviolet light). Upon defect detection, shafts were longitudinally cut in correspondence to the defect location. The obtained sections were polished in order to analyze fretting fatigue cracks. Cutting was performed by a miter saw equipped with emery discs. After that, to allow better handling, a longitudinal portion of the shaft was incorporated into a resin for each sample. The surface of the obtained cylindrical sample was sanded and polished in a lapping machine. For this purpose, sandpaper (grit from P80 to P2500) and cloth disks wetted by 0.05 μm alumina powder-water mixed were used. After the polishing task, fretting-induced crack paths, inclinations, and lengths were investigated by an Optiphot-100 optical microscope (by Nikon, Melville, NY, United States). Additional analyses were run by a Field Emission Gun Scanning Electron Microscope (SEM-FEG). This microscope (Mira3 Model, by TESCAN, Brno, Czech Republic) consists of a hot-cathode field emission gun (tungsten filament emitter) and energy-dispersive X-ray spectroscopy (EDS).

ITEM NO	PART NAME	MATERIAL	QTY
1	BUSHING	C40	1
2	HUB	39 NICRMO3	1
3	RING_NUT	39 NICRMO3	1
4	SHAFT	C40	1

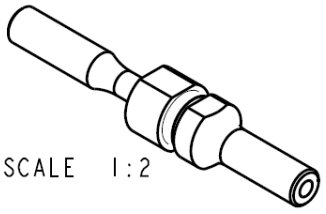

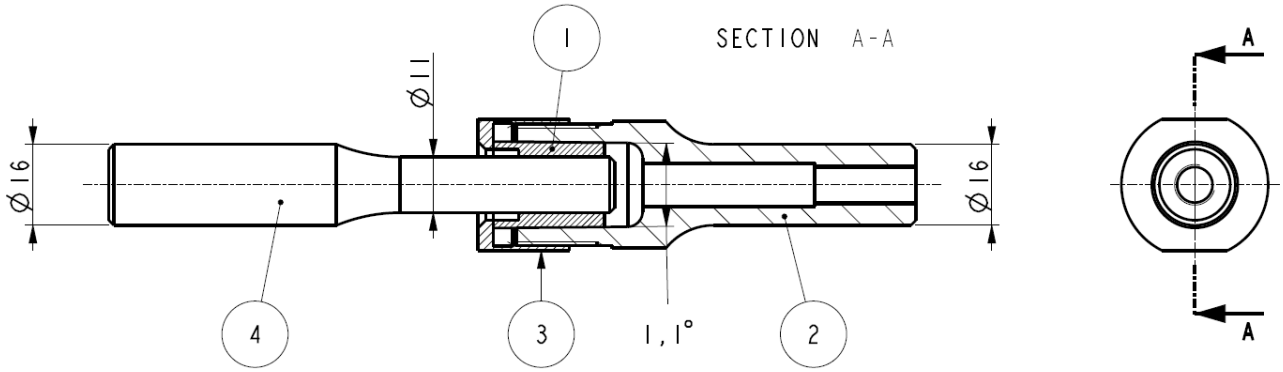

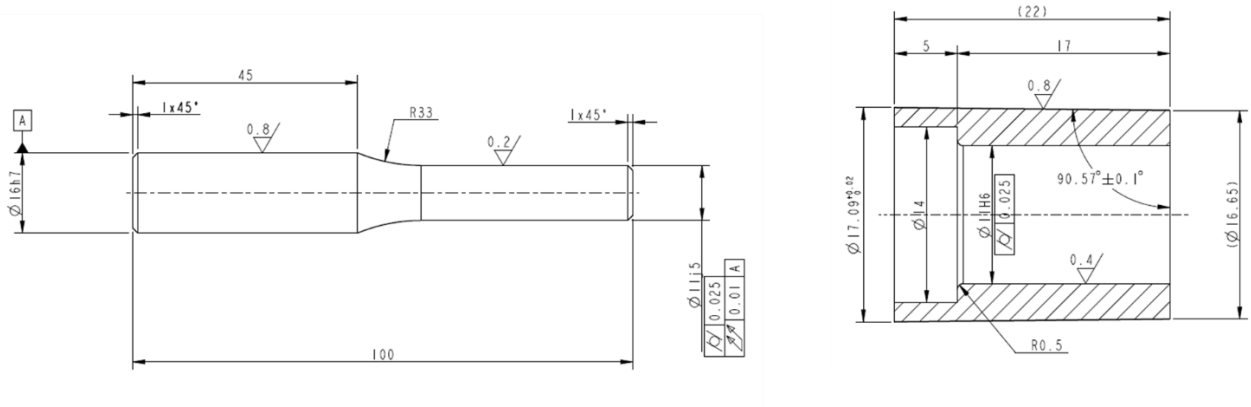

Figure 2 – Notched specimen assembly (not in scale, all dimensions in mm)

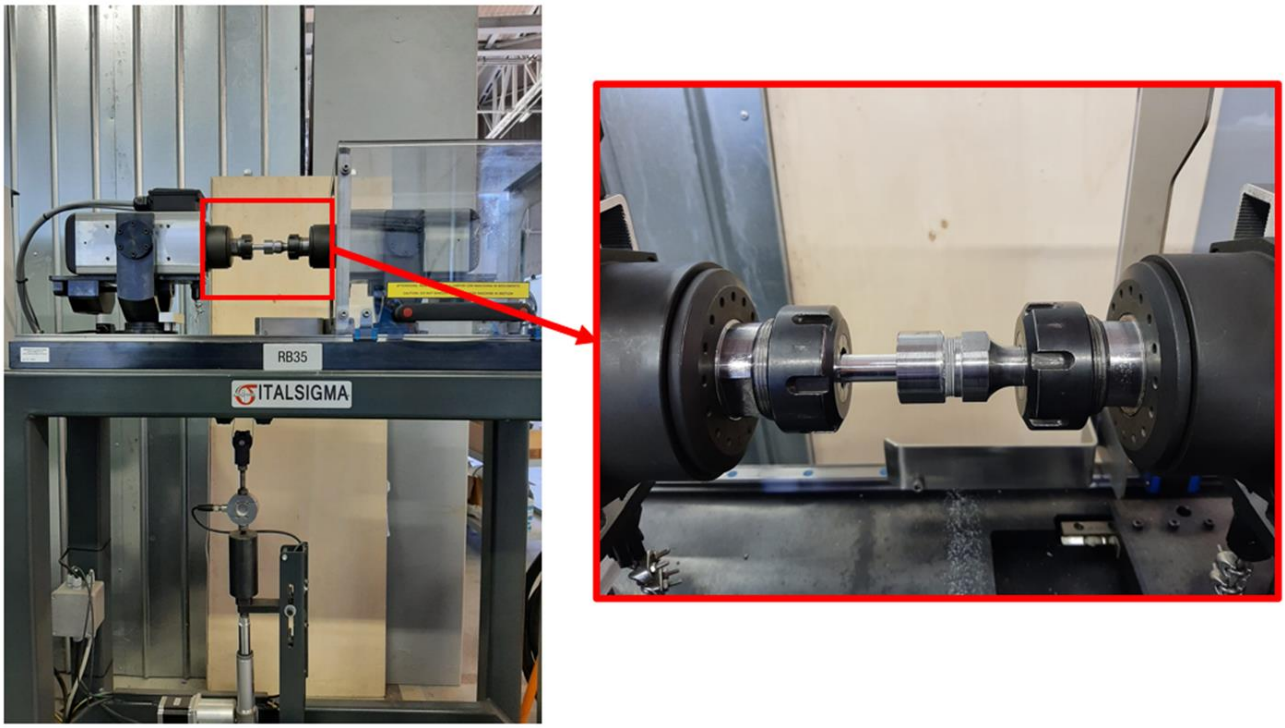

Figure 3 – Experimental setup

2.2 Contact pressure analytical model

The analytical model used to calculate the coupling pressure has been widely discussed in the literature [44,45]. The model is based on applying thick-wall cylinder theory, adapted to tapered couplings in this specific case. In this paper, we will report the most important formulas. We advise referring to the aforementioned references for a deeper understanding of the subject. Due to the

possible clearance between the bushing and the shaft, it may occur that before the related mating surfaces get in contact, the bushing needs to engage with the hub (upon the conical coupling) by a nonzero axial relative displacement. The actual pressure between the shaft and the bushing after the contact p_{BS} is yielded by Eq. 1, according to [44].

$$p_{BS} = \frac{\frac{z_{BS}}{r_{Se}} + \frac{p_{HB}}{E_B}\left(\frac{1+Q_H^{\,2}}{1-Q_H^{\,2}} + \nu_H\right) + \frac{1}{E_B}\left(\frac{1+Q_B^{\,2}}{1-Q_B^{\,2}} - \nu_B\right)}{\frac{1}{E_S}(1+\nu_S) + \frac{1}{E_B}\left(\frac{1+Q_B^{\,2}}{1-Q_B^{\,2}} - \nu_B\right)} \tag{1}$$

The resulting analytically computed contact pressure at the mating surfaces is plotted in Figure 4 for a diametral allowance of 14 μm, as a function of the relative displacement *s* between the bushing and the hub.

Figure 4 – Contact pressure at the mating surfaces as a function of the bushing-hub relative displacement *s*

In order to determine the tightening torque to be applied to the ring nut so that the desired contact pressure can be induced, an analytical model has been used. This model operates under the hypothesis that a lubricant (ceramic grease Interflon HT 1200) is applied to the threaded connection and at the

interface between the bushing and the hub. The rationale for this procedure is the lubricant provides a constant friction coefficient μ (steel to steel) of 0.12, based on the manufacturer datasheet [46].

Therefore, based on the desired coupling pressure, it was then possible to work out the introduction force Fi , complying with [45], as follows (Eq. 2):

$$Fi = p_{HB} \cdot A \cdot \cos\alpha \cdot \left(\tan\alpha + \mu_{BH}\right) \tag{2}$$

In this formula A indicates the actual contact area between the hub and the bushing and μ_{BH} is the friction coefficient at the conical interface between the bushing and the hub.

Thus, by Motosh's equations [47], the actual tightening torque T. can be determined as follows (Eq. 6):

$$T = Fi \cdot \left(0.16 \cdot p + 0.58 \cdot \mu_{th} \cdot d_2 + 0.5 \cdot \mu_b \cdot D_m\right) \tag{6}$$

Where p is the threaded pitch, μ_{th} is the friction coefficient in the threads, d_2 is the pitch diameter [48], μ_b is the bearing friction coefficient in the underhead, and D_m is the underhead mean diameter.

Provided the aforementioned lubricant was spread over all the surfaces, except for the coupling between the shaft and the bushing that was kept in dry conditions, a value of 0.12 was assumed for all the defined friction coefficients (μ_{BH}, μ_{th} and μ_b).

2.3 Experimental campaign

The specimen described above has then been involved in an experimental campaign to assess its relevant features and validate its capability of correctly reproducing the fretting fatigue mechanism. The shaft and the bushing were manufactured by C40 steel [49] (also referenced with the number 1.0511), whose chemical composition is reported in Table 1. The ring nut and the hub were instead

made of 39 NiCrMo 3 [50], thus making them reusable for multiple fatigue tests. The chemical composition of this material is provided in Table 2. The shaft and the bushing were changed after every test. Code SXX was assigned to each shaft, whereas code BXX was given to the bushing. The fatigue testing procedure was based on ISO 1143 Standard for rotating bending fatigue testing [43]. The Standard defines the testing procedure and the load scheme.

Table 1 – Chemical composition of C40 steel (wt%) [49]

C	**Si max**	**Mn**	**P max**	**S**	**Na max**	**Cr max**	**Mo max**	**Ni max**	**Cr+Mo+Ni Max**	**Others**
0.37 to 0.44	0.40	0.50 to 0.80	0.045	0.045	-	0.40	0.10	0.40	0.63	-

Table 2 – Chemical composition of 39 NiCrMo 3 (wt%) [50]

C	**Si max**	**Mn**	**P max**	**S max**	**Cr**	**Mo**	**Ni**	**V**	**B**
0.35 to 0.43	0.40	0.50 to 0.80	0.025	0.035	0.60 to 1.00	0.15 to 0.25	0.70 to 1.00	-	-

Every specimen underwent dimension and roughness checks to ensure they could meet the specifications in Figure 2. For the sake of synthesis, roughness measurements are not reported in this paper. Shaft-bushing specimens were arranged in pairs to minimize the scattering affecting the clearance value across the batch. The contact pressure at the coupling between the shaft and the bushing was set at 80 MPa.

The specimen dimensions, along with specimen pairs and clearance levels, are reported in Table 3. The tightening torque to achieve the desired contact pressure is also reported in the same Table.

Table 3 – Specimen couplings with clearance data

Shaft Nr.	Dimension [mm]	Bushing Nr.	Dimension [mm]	**Coupling**	Clearance [μm]	Tightening torque [Nm]
S01	11.0030	B21	11.0033	**S01/B21**	0.3	13.4
S09	11.0101	B02	11.0100	**S09/B02**	0.0	12.8
S07	11.0082	B06	11.0085	**S07/B06**	0.3	13.4
S18	11.0057	B25	11.0062	**S18/B25**	0.4	13.6
S27	11.0034	B22	11.0035	**S27/B22**	0.1	13.0
S13	11.0056	B10	11.0061	**S13/B10**	0.6	14.0

S19	11.0061	B27	11.0068	**S19/B27**	0.6	14.0
S11	11.0072	B19	11.0080	**S11/B19**	0.8	14.3
S05	11.0043	B14	11.0057	**S05/B14**	1.3	15.3
S26	11.0063	B23	11.0060	**S26/B23**	-0.3	12.2
S15	11.0117	B04	11.0119	**S15/B04**	0.2	13.2
S21	11.0138	B28	11.0138	**S21/B28**	0.0	12.8
S22	11.0130	B24	11.0131	**S22/B24**	0.1	13.0
S17	11.0108	B30	11.0113	**S17/B30**	0.5	13.8
S06	11.0118	B17	11.0125	**S06/B17**	0.7	14.2
S10	11.0155	B15	11.0164	**S10/B15**	0.9	14.5
S29	11.0103	B20	11.0113	**S29/B20**	1.0	14.7
S03	11.0093	B16	11.0105	**S03/B16**	1.2	15.1
S16	11.0088	B09	11.0103	**S16/B09**	1.5	15.7
S24	11.0098	B05	11.0114	**S24/B05**	1.6	15.9
S12	11.0088	B29	11.0106	**S12/B29**	1.8	16.3
S23	11.0075	B03	11.0096	**S23/B03**	2.1	16.8
S14	11.0055	B13	11.0078	**S14/B13**	2.3	17.2
S20	11.0060	B12	11.0088	**S20/B12**	2.8	18.2
S08	11.0065	B26	11.0099	**S08/B26**	3.4	19.3
S28	11.0063	B11	11.0097	**S28/B11**	3.4	19.3
S25	11.0023	B18	11.0115	**S25/B18**	9.2	30.4
S04	10.9945	B01	11.0114	**S04/B01**	16.9	45.1

All the specimens were tested by the aforementioned four-point rotating bending machine, where the sample was loaded under alternate load (load ratio, R=-1) with constant maximum bending moment [51,52]. In total, 29 pairs of specimens were tested with a rotating speed of 3,000 rpm. The run-out was set at 2,000,000 cycles following the Italian National Standard UNI 7670 (used mainly until a few years ago) and the original studies about fretting fatigue involving motorcycle forks [53]. This choice regarding runout does not compromise the outcomes regarding the proper applicability of the specimen. However, runout will be increased in the next studies on the topic in order to make it consistent with current recommendations. The fatigue testing was aimed at the determination of the fatigue limit. A staircase method was applied for this purpose according to Standard ISO 12107 [54]. Following the tests, the fracture surfaces along with the cylindrical surface of the shafts (involving both failed and survived specimens) were carefully analyzed by a stereoscopic microscope (Stemi 305 by ZEISS, Oberkochen, Germany), in order to detect the crack initiation point and to assess the occurrence of fretting. It is worth mentioning that some additional trials have been run: in these tests,

specimens were fatigued up to a number of cycles being significantly lower than the predicted number of cycles to failure. The fatigue life estimation was made based on the S-N curve reported in [41]. After these tests, the specimens were disassembled, and, in order to detect the plane where crack initiation had reasonably occurred, a dye penetrant inspection was carried out on the shaft (Figure 5), as described above. Post-emulsifiable fluorescent penetrants were used for this purpose. The crack initiation sites and the planes involving crack propagation paths were reasonably determined through sample examination in a dark room. Afterwards, the shafts were longitudinally cut along these planes by standard metallographic techniques.

Figure 5 – Dye penetration inspection on the shaft specimens

3. Results and discussion

The experimental fatigue results are reported in Table 4. The table provides sample identification, maximum nominal bending stress (corresponding to the stress amplitude) at the gage, and the number of cycles to failure. Finally, in the last column, an indication of the trial outcome (Runout or failure)

is provided. In particular, “Run out” indicates that the specimen survived up to $2 \cdot 10^6$ cycles and that the test was consequently stopped, whereas “Yes” indicates failed specimens.

Table 4 – Results of the fatigue tests

Specimen	Stress (S) [MPa]	Life cycles (N)	Failure
S01/B21	210	2,000,000	Run out
S09/B02	269	559,724	Yes
S07/B06	250	1,075,722	Yes
S18/B25	230	578,533	Yes
S27/B22	220	2,000,000	Run out
S13/B10	230	2,000,000	Run out
S19/B27	240	514,006	Yes
S11/B19	230	2,000,000	Run out
S05/B14	240	2,000,000	Run out
S26/B23	240	380,710	Yes
S15/B04	230	2,000,000	Run out
S21/B28	240	2,000,000	Run out
S22/B24	250	423,275	Yes
S17/B30	240	3,937,199	Yes
S06/B17	250	2,000,000	Run out
S10/B15	260	351,847	Yes
S29/B20	250	2,000,000	Run out

The experimental results were processed to obtain the fatigue limit of the notched specimens in agreement with Standard [54]. The application of the staircase method yielded a fatigue limit $S_{n\_notched} = 254$ MPa with a standard deviation $\sigma_{notched} = 10$ MPa. Comparing this result with the endurance limit (50% at $5 \cdot 10^6$ cycles) of plain specimens indicated in [41] ($S_{n\_plain} = 364$ MPa and $\sigma_{plain} = 6$ MPa), the stress concentration factor for fatigue (notch factor) given by the interference joint may be determined.

$$k_f = \frac{S_{n\_plain}}{S_{n\_notched}} = 1.43 \tag{4}$$

Two examples of fracture surfaces of shaft specimens are shown in Figure 6. The circle and the arrow indicate the zone of the final fracture. The extension of the relevant zones of final fracture is compliant with specimen load history. The multiple crack initiation sites on the surface are consistent with a steep stress gradient at the end of the bushing radius [51,52].

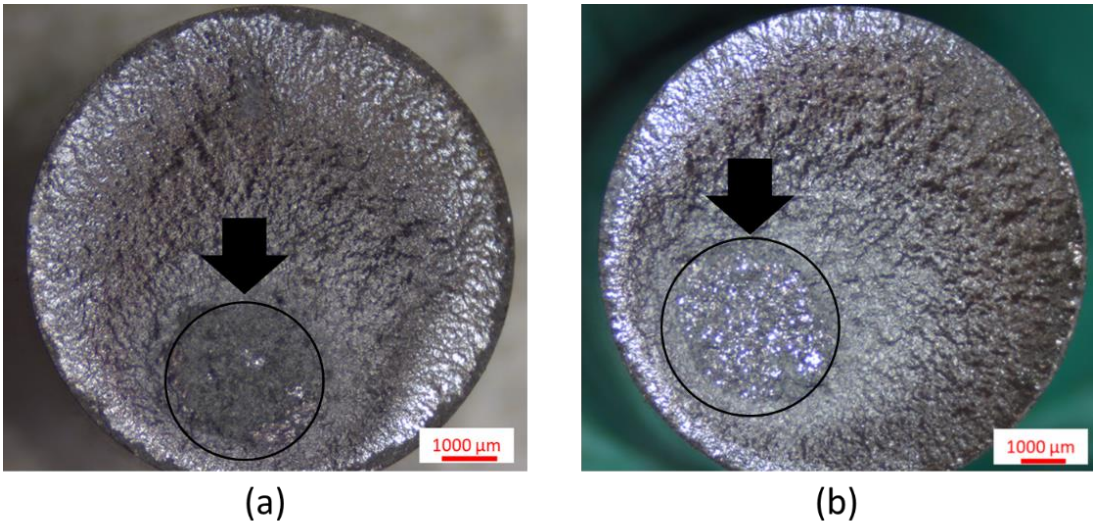

Figure 6 – Specimen fracture surfaces (a) S07 failed at 1,075,722 cycles, and (b) S09 failed at 559,724 cycles

Typical contact surfaces after the test are shown in Figure 7: the presence of iron oxides at the bushing end mating suggests the presence of fretting damage [40,55]. Moreover, the amount of oxidated area in the vicinity of the contact point between the shaft and the bushing bore radius in the axial direction is in the order of 0.5 mm.

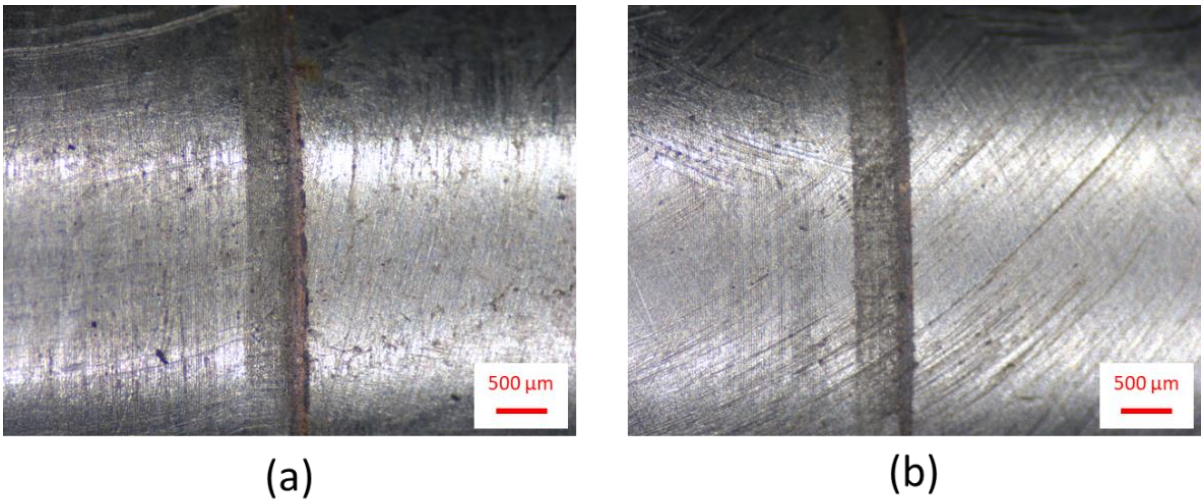

Figure 7 – Cylindrical surface of the shafts at the bushing end contact after test (a) S06 (outcome: run out), and (b) S29 (outcome: run out)

Table 5 – Interrupted fatigue tests

Specimen	Stress (S) [MPa]	Life cycles (N)
S03/B12	269	400,000
S16/B09	269	400,000
S24/B05	269	400,000
S18/B25	269	400,000
S12/B29	269	400,000
S23/B03	269	400,000
S14/B13	269	400,000
S20/B12	269	400,000
S08/B26	269	400,000
S28/B11	269	400,000
S25/B18	269	400,000
S04/B01	269	400,000

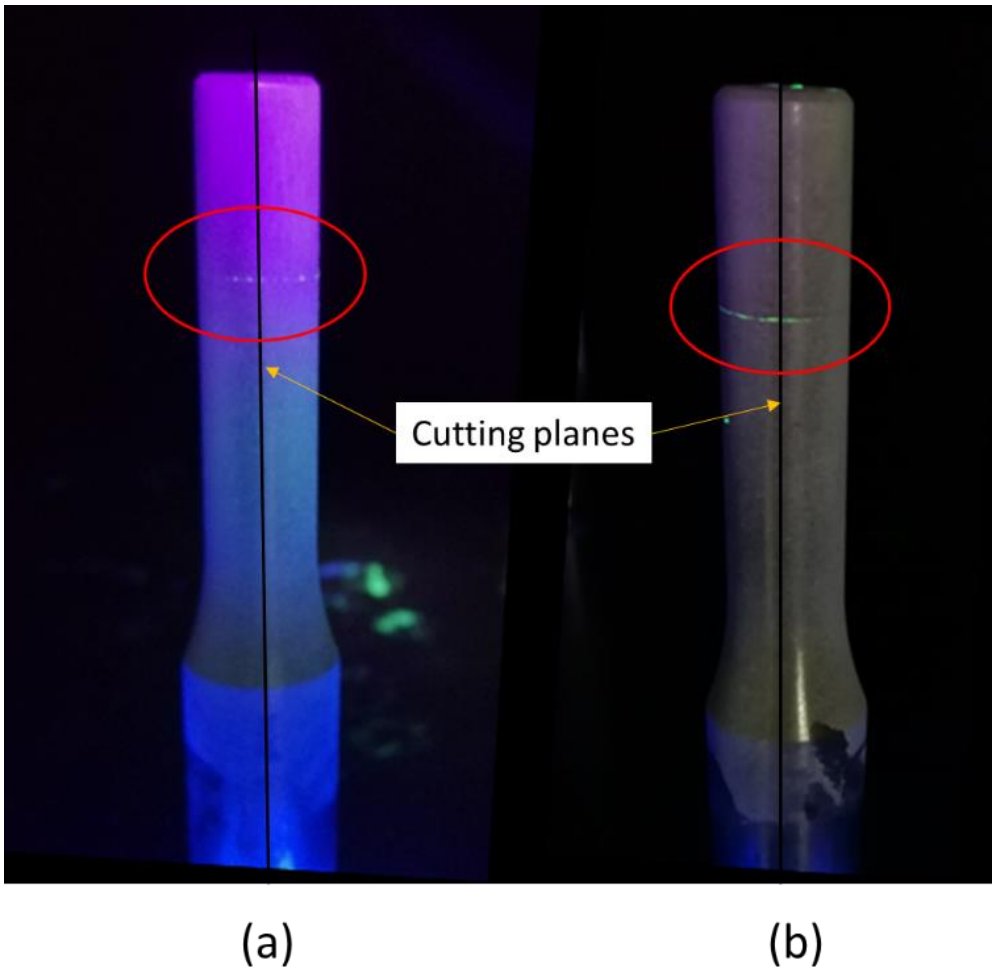

Figure 8 – Dye penetrant inspection on the specimens (a) S25 (test stopped after 400,000 cycles) and (b) S24 (as above)

The results of the interrupted fatigue tests, which involved specimens loaded under the maximum achievable stress amplitude by the rotating bending testing machine, are reported in Table. 5. As above, fluorescent dye penetrant inspection was performed for all the samples but, for the sake of synthesis, just the outcomes for two shaft specimens (S24 and S25) are shown in Figure 8. A long fatigue crack with several initiation points at the surface is highlighted in both samples at the fretted region. Therefore, the shafts were cut along longitudinal axes (i.e., along main axes of inertia), as highlighted in Figure 8 to observe the aforementioned region by an optical microscope. Typical views along longitudinal sections are displayed in Figures 9 to 11. The latter contains a detail of the crack

in Figure 11, whose layout was highlighted by SEM-FEG observation. It must be remarked that, due to the multiaxial stress state, the fretting cracks do not grow in the radial direction. The observed crack orientation is slanted by an angle between 0° and 45° due to the shear stress on the sample surface. The crack orientation angle, which always propagates inside the coupling, is higher near the surface than inside the sample. A possible reason for this outcome is that the contribution of shear stresses tends to decrease for inner layers, and conversely, the contribution by bending-induced normal (longitudinal) stresses increases. Therefore, the greater depth, the lower the crack inclination (until they become radial). Furthermore, alongside the main crack, there are minor secondary cracks. These outcomes are completely aligned with those reported in the literature dealing with fretting fatigue [55]. Therefore, it must be pointed out that these results indicate that the developed specimen, whose design was supported by the aforementioned analytical model, can properly replicate the fretting phenomenon in shaft-hub joints with interference. In fact, the specimen proved to enable accurate coupling pressure control (which is not possible with a more conventional shaft-hub interference fitted joint). Moreover, as it has been observed, fatigue testing by this specimen can reproduce fretting mechanisms and damage. Quantitative results may also be determined regarding fatigue strength and life, wear width and crack inclination and path. This achievement is made possible by the particular feature of the specimen that can be disassembled without scratching the mating surfaces, particularly those involved by wear as an effect of relative displacement. Consequently, thorough microscope analyses may be run.

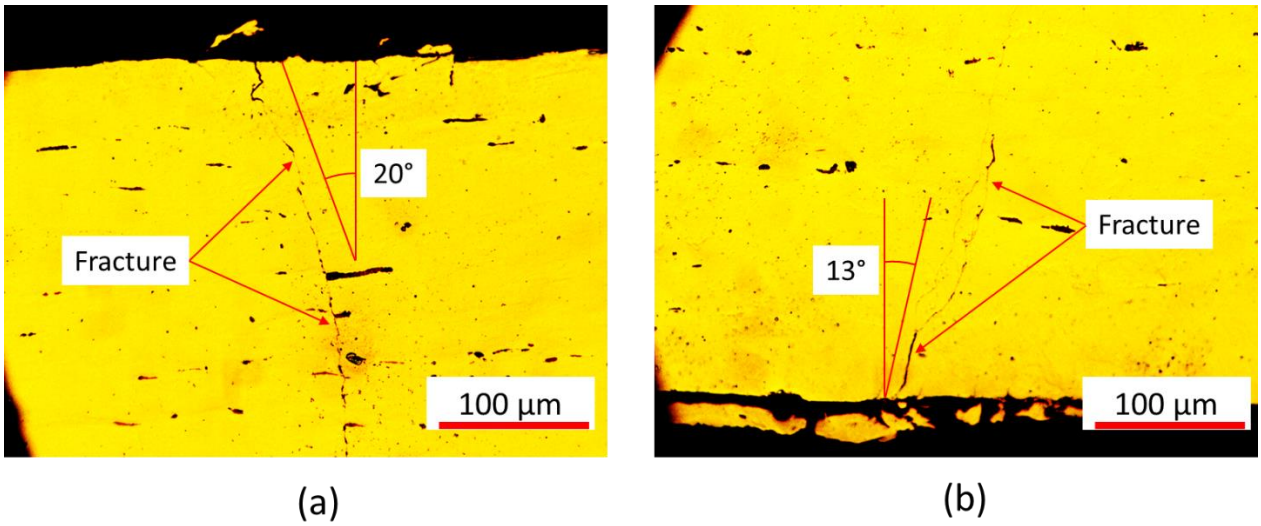

Figure 9 –Sectional view (shaft longitudinal section) of two different cracks (a) and (b) on shaft S25 (bushing on the right side)

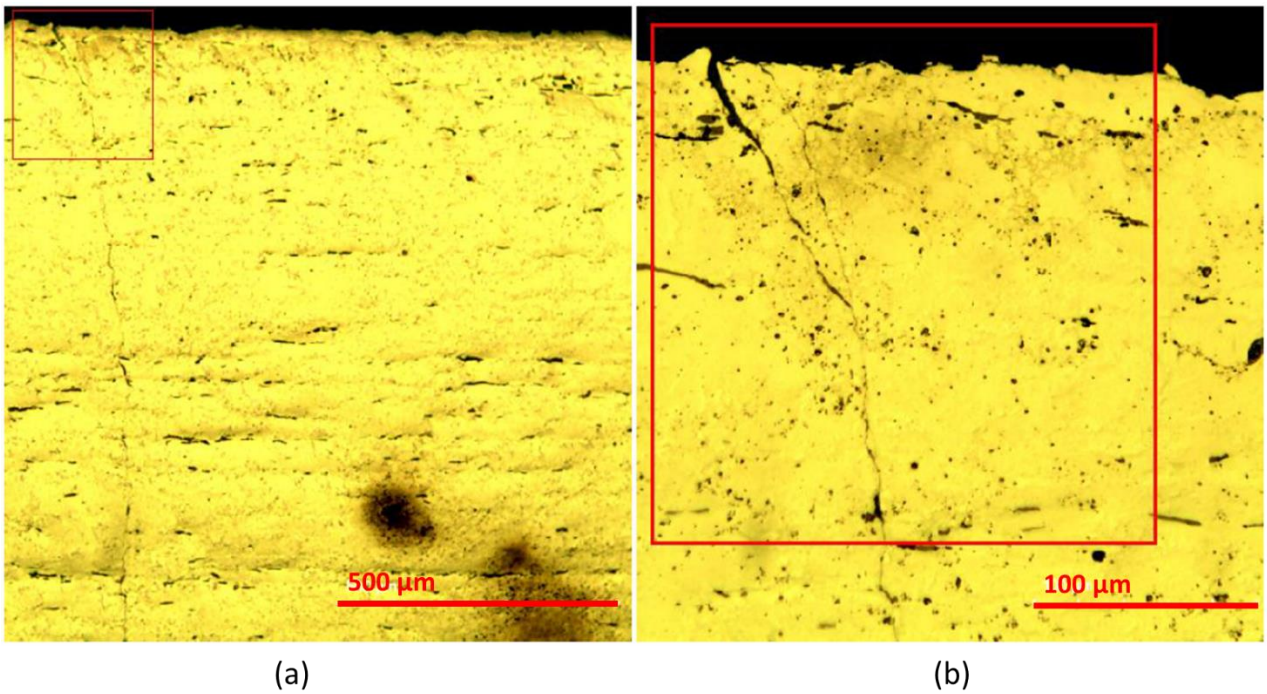

Figure 10 –Sectional view (shaft longitudinal section) of a crack on shaft S24: (a) lower magnification and (b) higher magnification

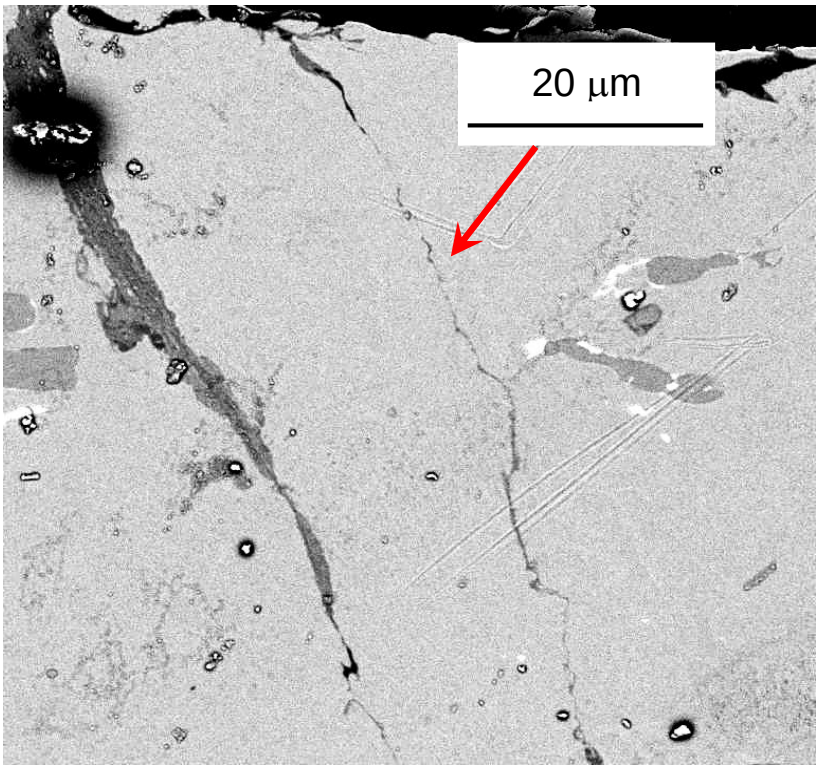

Figure 11 –A detail of the crack path (shaft S24) examined by SEM-FEG and here highlighted by an arrow

4. Conclusions

In this study, the effect of fretting on the fatigue behavior of an interference-fitted joint was analyzed. First, a customized specimen was designed to enable control of the actual contact pressure between the mating surfaces. This specimen, taking advantage of a conical coupling, makes it possible to control the contact pressure at the mating surfaces of the shaft and the hub with a good confidence level. The same specimen has the remarkable feature of enabling decoupling after fatigue cycling without damaging the mating surfaces. This point is a crucial issue, considering the common need for specimen surface microscope observation and fretting damage and fretting-induced crack initiation site detection.

The specimen suitability for fretting fatigue-related problems has been validated by experimental tests. The experimental campaign involved C40 steel that was tested according to the ISO Standard on a four-point rotating bending machine. The specimens were accurately checked in terms of

dimensions and roughness in order to assess their compliance with the technical drawing. After that, the specimens were sorted out in pairs to keep the clearance/interference level as constant as possible. The assembly was carried out by applying a tightening torque that was analytically evaluated for a target contact pressure of 80 MPa. Seventeen specimens were tested as a total in order to determine the fretting fatigue limit of 254 MPa for the notched specimens by Staircase Method. It was then also possible to evaluate the fatigue strength reduction factor for this experimental setup, which turned out to be equal to 1.43. In addition, twelve specimens were tested under the maximum load achievable by the test bench, but in this case, the tests were interrupted before the expected life to failure.

This procedure made it possible to analyze wear at the shaft mating surfaces by stereoscopic microscope and then to detect crack initiation sites by fluorescent penetrant liquids. The shafts were then properly cut to highlight crack paths by subsequent microscope observation. It was assessed that the cracks were not perpendicular to the shaft axes in agreement with the relevant literature about fretting fatigue. They appear to be slanted up to an inclination of 45° at the surface as an effect of fretting-induced shear stresses.

These results prove that the developed specimen can reliably replicate the fretting phenomenon in shaft-hub joints with interference. Therefore, it makes it possible to make qualitative and quantitative evaluations related to wear and cracking, depending on coupling pressure at the shaft-hub interface. Since the relative displacement in this kind of coupling is minimal, this specimen can also help with the understanding of the fretting behavior of a material for almost zero relative displacements ($< 10\mu m$). It is worth mentioning it is nowadays very difficult to address this problem with traditional fretting pad-testing machines.

For this set of studies, a run-out at 2,000,000 cycles was set, following the old national standard UNI 7670. This choice regarding runout does not compromise the outcomes regarding the proper applicability of the specimen. However, runout will be increased in the next studies on the topic in order to make it consistent with current recommendations.

References

[1] D. Croccolo, M. De Agostinis, N. Vincenzi, Recent improvements and design formulae applied to front motorbike suspensions, Eng. Fail. Anal. 17 (2010) 1173–1187. https://doi.org/10.1016/j.engfailanal.2010.02.002.

[2] A. Strozzi, A. Baldini, M. Giacopini, E. Bertocchi, L. Bertocchi, Normalization of the stress concentrations at the rounded edges of a shaft-hub interference fit, J. Strain Anal. Eng. Des. 46 (2011) 478–491. https://doi.org/10.1177/0309324711403845.

[3] D. Croccolo, M. De Agostinis, N. Vincenzi, Normalization of the stress concentrations at the rounded edges of a shaft-hub interference fit: Extension to the case of a hollow shaft, J. Strain Anal. Eng. Des. 47 (2012) 131–139. https://doi.org/10.1177/0309324712439982.

[4] H. Shelton, J.O. Sullivan, K. Gall, Analysis of the fatigue failure of a mountain bike front shock, Eng. Fail. Anal. 11 (2004) 375–386. https://doi.org/10.1016/j.engfailanal.2003.06.002.

[5] F. Kolonits, Fretting in a hub-axle press fit joint, in: Proc. Mini Conf. Veh. Syst. Dyn. Identif. Anomalies, 2006: pp. 573–583.

[6] M. Madia, S. Beretta, U. Zerbst, An investigation on the influence of rotary bending and press fitting on stress intensity factors and fatigue crack growth in railway axles, Eng. Fract. Mech. 75 (2008) 1906–1920. https://doi.org/10.1016/j.engfracmech.2007.08.015.

[7] G. Gürer, C.H. Gür, Failure analysis of fretting fatigue initiation and growth on railway axle press-fits, Eng. Fail. Anal. 84 (2018) 151–166. https://doi.org/10.1016/j.engfailanal.2017.06.054.

[8] C. Song, M.X. Shen, X.F. Lin, D.W. Liu, M.H. Zhu, An investigation on rotatory bending fretting fatigue damage of railway axles, Fatigue Fract. Eng. Mater. Struct. 37 (2014) 72–84.

https://doi.org/10.1111/ffe.12085.

[9] G. Olmi, Low cycle fatigue experiments on turbogenerator steels and a new method for defining confidence bands, J. Test. Eval. 40 (2012). https://doi.org/10.1520/JTE104548.

[10] E. Masoumi Khalil Abad, G.H. Farrahi, M. Masoumi Khalil Abad, A.A. Zare, S. Parsa, Failure analysis of a gas turbine compressor in a thermal power plant, J. Fail. Anal. Prev. 13 (2013) 313–319. https://doi.org/10.1007/s11668-013-9663-8.

[11] M. Fonte, M. Freitas, L. Reis, Failure analysis of a damaged diesel motor crankshaft, Eng. Fail. Anal. 102 (2019) 1–6. https://doi.org/10.1016/j.engfailanal.2019.04.025.

[12] K. Anandavel, R. V. Prakash, Effect of three-dimensional loading on macroscopic fretting aspects of an aero-engine bladedisc dovetail interface, Tribol. Int. 44 (2011) 1544–1555. https://doi.org/10.1016/j.triboint.2010.10.014.

[13] J. Ding, W.S. Sum, R. Sabesan, S.B. Leen, I.R. McColl, E.J. Williams, Fretting fatigue predictions in a complex coupling, Int. J. Fatigue. 29 (2007) 1229–1244. https://doi.org/10.1016/j.ijfatigue.2006.10.017.

[14] D.S. Wei, L. Shi, Y.R. Wang, Cyclic plastic behavior of dovetail under fretting load, Eng. Fail. Anal. 55 (2015) 100–114. https://doi.org/10.1016/j.engfailanal.2015.05.009.

[15] D.S. Wei, S.H. Yuan, Y.R. Wang, Failure analysis of dovetail assemblies under fretting load, Eng. Fail. Anal. 26 (2012) 381–396. https://doi.org/10.1016/j.engfailanal.2012.06.007.

[16] L. Shi, D.S. Wei, Y.R. Wang, A.M. Tian, D. Li, An investigation of fretting fatigue in a circular arc dovetail assembly, Int. J. Fatigue. 82 (2016) 226–237. https://doi.org/10.1016/j.ijfatigue.2015.07.025.

[17] Q. Yang, W. Zhou, P. Gai, X. Zhang, X. Fu, G. Chen, Z. Li, Investigation on the fretting fatigue behaviors of Ti-6Al-4V dovetail joint specimens treated with shot-peening, Wear. 372–373

(2017) 81–90. https://doi.org/10.1016/j.wear.2016.12.004.

[18] D. Mangardich, F. Abrari, Z. Fawaz, A fracture mechanics based approach for the fretting fatigue of aircraft engine fan dovetail attachments, Int. J. Fatigue. 129 (2019) 105213. https://doi.org/10.1016/j.ijfatigue.2019.105213.

[19] P.J. Golden, Development of a dovetail fretting fatigue fixture for turbine engine materials, Int. J. Fatigue. 31 (2009) 620–628. https://doi.org/10.1016/j.ijfatigue.2008.03.017.

[20] D.-K. Zhang, H. Geng, Z.-F. Zhang, D.-G. Wang, S.-Q. Wang, S.-R. Ge, Investigation on the fretting fatigue behaviors of steel wires under different strain ratios, Wear. 303 (2013) 334–342. https://doi.org/10.1016/j.wear.2013.03.020.

[21] G.A. Tomlinson, The rusting of steel surfaces in contact, Proc. Roy. Soc.,. 115 (1927) 472-483.

[22] D. Kumar, R. Biswas, L.H. Poh, M.A. Wahab, Fretting fatigue stress analysis in heterogeneous material using direct numerical simulations in solid mechanics, Tribol. Int. 109 (2017) 124–132. https://doi.org/10.1016/j.triboint.2016.12.033.

[23] D. Infante-García, E. Giner, H. Miguélez, M. Abdel Wahab, Numerical analysis of the influence of micro-voids on fretting fatigue crack initiation lifetime, Tribol. Int. 135 (2019) 121–129. https://doi.org/10.1016/j.triboint.2019.02.032.

[24] T. Yue, M. Abdel Wahab, Finite element analysis of fretting wear under variable coefficient of friction and different contact regimes, Tribol. Int. 107 (2017) 274–282. https://doi.org/10.1016/j.triboint.2016.11.044.

[25] B. Zeise, R. Liebich, M. Prölß, Simulation of fretting wear evolution for fatigue endurance limit estimation of assemblies, Wear. 316 (2014) 49–57. https://doi.org/10.1016/j.wear.2014.04.013.

[26] K. Fan, D. Liu, X. Zhang, D. Liu, W. Zhao, J. Yang, A. Ma, M. Li, Y. Qi, J. Xiang, M. Abdel Wahab, Effect of residual stress induced by ultrasonic surface rolling on fretting fatigue behaviors of Ti-6Al-4V alloy, Eng. Fract. Mech. 259 (2022). https://doi.org/10.1016/j.engfracmech.2021.108150.

[27] M.C. Gaspar, A. Ramalho, Fretting behaviour of galvanised steel, Wear. 252 (2002) 199–209. https://doi.org/10.1016/S0043-1648(01)00874-2.

[28] T. Christiner, J. Reiser, I. Gódor, W. Eichlseder, F. Trieb, R. Stühlinger, The fatigue endurance limit of a high strength CrNi steel in a fretting dominated regime, Tribol. Int. 59 (2013) 97–103. https://doi.org/10.1016/j.triboint.2012.01.014.

[29] G.Z. Xu, J.J. Liu, Z.R. Zhou, Prediction of the fretting fatigue resistance of various surface-modification layers on 1045 steel: The role of fretting maps, Tribol. Int. 34 (2001) 569–575. https://doi.org/10.1016/S0301-679X(01)00057-3.

[30] L. Ma, K. Eom, J. Geringer, T. Jun, Literature Review on Fretting Wear and Contact Mechanics of Tribological Coatings, (n.d.) 1–20.

[31] S.L. Sunde, B. Haugen, F. Berto, Experimental and numerical fretting fatigue using a new test fixture, Int. J. Fatigue. 143 (2021). https://doi.org/10.1016/j.ijfatigue.2020.106011.

[32] P.J. Golden, A.L. Hutson, B.B. Bartha, T. Nicholas, Fatigue loading and life prediction in three fretting fatigue fixtures, Exp. Mech. 48 (2008) 253–263. https://doi.org/10.1007/s11340-008-9130-8.

[33] K. Nishioka, S. Nishimura, K. Hirakawa, Fundamental Investigations of Fretting Fatigue : Part 1,On the Relative Slip Amplitude of Press-fitted Axle Assemblies, Bull. JSME. 11 (1968) 437–445.

[34] M. Luke, I. Varfolomeev, K. Lütkepohl, A. Esderts, Fatigue crack growth in railway axles: Assessment concept and validation tests, Eng. Fract. Mech. 78 (2011) 714–730.

https://doi.org/10.1016/j.engfracmech.2010.11.024.

[35] D. Croccolo, M. De Agostinis, S. Fini, G. Olmi, F. Robusto, C. Sca-, Fretting fatigue in mechanical joints : a literature review, (2022) 1–44.

[36] K. Hirakawa, K. Toyama, M. Kubota, The analysis and prevention of failure in railway axles, Int. J. Fatigue. 20 (1998) 135–144. https://doi.org/10.1016/S0142-1123(97)00096-0.

[37] T. Juuma, Torsional fretting fatigue strength of a shrink-fitted shaft, Wear. 231 (1999). https://doi.org/10.1016/S0301-679X(00)00102-X.

[38] V. Linhart, I. Černý, An effect of strength of railway axle steels on fatigue resistance under press fit, Eng. Fract. Mech. 78 (2011) 731–741. https://doi.org/10.1016/j.engfracmech.2010.11.023.

[39] B. Alfredsson, Fretting fatigue of a shrink-fit pin subjected to rotating bending: Experiments and simulations, Int. J. Fatigue. 31 (2009) 1559–1570. https://doi.org/10.1016/j.ijfatigue.2009.04.019.

[40] Y. Zhang, L. Lu, Y. Gong, J. Zhang, D. Zeng, Fretting wear-induced evolution of surface damage in press-fitted shaft, Wear. 384–385 (2017) 131–141. https://doi.org/10.1016/j.wear.2017.05.014.

[41] D. Croccolo, M. De Agostinis, G. Olmi, Fatigue life characterisation of interference fitted joints, in: ASME Int. Mech. Eng. Congr. Expo. Proc., 2013. https://doi.org/10.1115/IMECE2013-63515.

[42] D. Croccolo, M. De Agostinis, S. Fini, A. Morri, G. Olmi, Analysis of the influence of fretting on the fatigue life of interference fitted joints, in: ASME Int. Mech. Eng. Congr. Expo. Proc., 2014. https://doi.org/10.1115/IMECE2014-38128.

[43] ISO 1143 : 2010, Metallic materials — Rotating bar bending fatigue testing, (2010).

[44] D. Croccolo, N. Vincenzi, A generalized theory for shaft-hub couplings, Proc. Inst. Mech. Eng. Part C J. Mech. Eng. Sci. 223 (2009) 2231–2239. https://doi.org/10.1243/09544062JMES1437.

[45] G. Niemann, Machine elements: design and calculation in mechanical engineering, Springer, Berlin, 1978.

[46] Interflon Paste HT1200, (2022).

[47] N. Motosh, Load distribution on threads of titanium tension nuts and steel bolts, J. Manuf. Sci. Eng. Trans. ASME. 97 (1975) 162–166. https://doi.org/10.1115/1.3438531.

[48] ISO 68-1:1998, ISO general purpose metric screw threads — Basic profile, (1998).

[49] EN 10277-2, Bright steel products - Technical delivery conditions, Part 2 Steels Gen. Eng. Purp. EN 10277 (2008).

[50] EN 10083-3, Steels for quenching and tempering, 3 (2006).

[51] D. Croccolo, M. De Agostinis, S. Fini, G. Olmi, F. Robusto, Coating effect on the fatigue strength of a free cutting steel, Proc. Inst. Mech. Eng. Part C J. Mech. Eng. Sci. 233 (2019) 7513–7524. https://doi.org/10.1177/0954406219836441.

[52] D. Croccolo, M. De Agostinis, S. Fini, G. Olmi, F. Robusto, S. Ciric-Kostic, A. Vranic, N. Muharemovic, N. Bogojevic, Fatigue response of as built DMLS processed Maraging Steel and effects of machining and heat and surface treatments, in: 2018.

[53] F. Berto, D. Croccolo, R. Cuppini, Fatigue strength of a fork-pin equivalent coupling in terms of the local strain energy density, 29 (2008) 1780–1792. https://doi.org/10.1016/j.matdes.2008.03.031.

[54] ISO 12107, Metallic materials - Fatigue testing - Statistical planning and analysis of data, 2012.

[55] K. Nishioka, K. Hirakawa, Fundamental investigation of fretting fatigue Part 3: some

phenomena and mechanism of surface cracks, Bull. JSME. 12 (1969) 397–407.